Total cross-section calculations on proton-impact ionization of hydrogen

Emil Y. Sidky and C. D. Lin
Department of Physics, Cardwell Hall, Kansas State University, Manhattan, Kansas 66506
(Received 14 May 2001; published 14 December 2001)

We have calculated the total cross section for proton-impact ionization of atomic hydrogen for the intermediate energy range 25–100 keV. We evaluate error bars of 5% on our theoretical values. The present results disagree with the experiment of Shah and Gilbody [J. Phys. B **14**, 2361 (1981)] and Shah *et al.* [J. Phys. B **20**, 2481 (1987)], differing by 20% at the peak of the ionization cross section. On the other hand, our results show better agreement with two recent theoretical calculations, one performed by close coupling and the other by integrating the time-dependent Schrödinger equation on a three-dimensional lattice. The present results also compare favorably with theoretical and experimental determinations of capture and excitation cross sections. We describe the two-center momentum space discretization method, used here, in detail, explaining how the cross sections and corresponding error bars are determined.

DOI: 10.1103/PhysRevA.65.012711 PACS number(s): 34.50.Fa, 31.15.Ar, 34.10.+x

I. INTRODUCTION

Ion impact ionization has been an interesting problem for many years, but most recently, there has been a flurry of work on the subject of proton impact ionization of molecules with the aim of understanding radiation damage in biological systems [1,2]. Unfortunately, our understanding of even the most basic ion impact collision system, protons on hydrogen, is not very good. At the peak of the ionization cross section, numbers available from the ''best'' experiment [3,4] and ''best'' theory [5] disagree by 20%.

The proton-hydrogen system is a prototype for ion-atom collision systems. The theoretical understanding of ion-atom collisions is based on methods and models tried out on this fundamental collision system. Yet, a complete description of proton-hydrogen collisions at keV energies has proved elusive. The basic reaction channels are elastic scattering, target excitation, capture to the projectile and ionization. Ionization is the least understood process of the four. In the intermediate energy regime 25–100 keV, where the projectile proton comes in at a speed comparable to the average speed of the electron, all four processes are important and interconnected. A poor understanding of one – ionization – limits the accuracy of the description of all other processes. Thus, it is paramount to develop a theoretical description of electron ejection in the proton-hydrogen system that can give the total ionization cross section to arbitrary accuracy.

The first *ab initio* attempt at computing the total ionization cross section at intermediate impact energies was performed by Shakeshaft [6]. He employed a two-center expansion in atomic orbitals about both centers, using pseudostates (positive energy, localized states) to represent the ionization continuum. At the time, Shakeshaft's calculation came in at 20% below the maximum for ionization total cross section from available experimental data. Later, measurements by Shah and Gilbody and Shah *et al.* [3,4] were in better agreement with the calculation of Ref. [6]. Further elaboration of the two-center atomic orbitals method by Kuang and Lin [7,8] showed very good agreement between theory and the experiment of Shah *et al.* in the intermediate impact energy range. The issue seemed to be settled until Toshima [5] performed a very detailed study of the two-center close-coupling method and determined that previous close-coupling studies were not converged. His studies provided cross sections that were now 20% higher than the experiment of Shah *et al.* Lattice calculations by Kolakowska *et al.* [9] came in also significantly higher than the experiment at the maximum of the ionization cross section. Thus, the present situation is the opposite of what it was in 1978; the theory now predicts 20% higher-ionization cross sections than the experiment measures.

Experimentally, the proton-hydrogen collision system is difficult to investigate because of problems in making and characterizing the atomic hydrogen target. The first studies by Fite *et al.* [10] measured the ionization cross section up to an impact energy of 40 keV, but the error bars were at the 20–30 % level. Other early measurements made by Gilbody and Ireland [11] and Park *et al.* [12] in the intermediate impact energy regime also had a large experimental error. The generally accepted numbers for the total ionization cross section in p-H collisions were generated from experiments done by Shah and Gilbody and Shah *et al.* in 1981 and 1987 [3,4], which claim experimental error on the level of 5% or better. Recent studies by Kerby *et al.* [13], focusing on the doubly differential cross section for ejecting electrons in the p-H system, produced total ionization cross sections, which differ from Refs. [3,4] by up to 29%.

On the theoretical side, there is much more work done on the proton-hydrogen collision system, see Refs. [14,15] and references therein. The reason for this is obvious; the p-H system contains only one electron and a simple Coulomb interaction with the two protons, the motion of which may be described classically to a good approximation. Thus, the p-H system reduces to the quantum-mechanical study of a single electron in the time-dependent field of two moving protons. As a result, most elastic and inelastic processes involving bound states on the target or projectile protons are well described by current theory.

Ionization, however, remains a challenge even for the p-H system. Within the last five years, a variety of approaches for obtaining the ionization total cross section in proton-hydrogen collision have appeared in the literature (in reverse

TABLE I. Ionization and other inelastic cross sections in units of 10^{-16} cm^2. All numbers have 5% error.

E (keV)	Ionization	Excitation $2s$	Excitation $2p$	Capture $2s$	Capture $2p$
25	0.961	0.1423	0.5103	0.3994	0.1956
40	1.649	0.1566	0.6266	0.2262	0.0815
50	1.801	0.1464	0.6587	0.1384	0.0447
75	1.700	0.1151	0.7078	0.0412	0.0109
100	1.457	0.0931	0.7124	0.0144	0.0033

chronological order): Finite Hilbert basis set calculations by Fu *et al.* [16], classical trajectory Monte Carlo calculations with initial ensemble geared for ionization [17], direct solution of the time-dependent Schrödinger equation on a very large three-dimensional lattice [9], an extensive study of the two-center close-coupling approach by Toshima [5], perturbation theory using a time-dependent two-state model as a zeroth order trial wave function [18], and a three-center close-coupling calculation by McLaughlin *et al.* [15]. In this paper, we will discuss at length the close-coupling method and the lattice calculation in comparison with the present calculation.

To address the issue of ionization in proton-hydrogen collisions, we have developed the two-center momentum space discretization (TCMSD) method [19,20]. The original purpose of the TCMSD method was to examine the full three-dimensional distribution of ejected electrons, and we have applied the method to understand the saddle-point mechanism in low-velocity proton-hydrogen collisions [21] and α-H collisions [22]. For the low-impact velocities, the TCMSD method cannot propagate the electronic wave function far enough to establish a final probability of ionization. On the other hand, for impact velocities 1 a.u. and above, the TCMSD method may reach large enough times to give a total ionization cross section. Moreover, TCMSD allows us to put error bars on our computed numbers. In this paper, we first show the TCMSD results for inelastic processes in proton-hydrogen collisions, then we give a detailed account of the theory with the parameters used in the current calculation and finally, we discuss the convergence of our calculation relative to other theoretical work.

II. INELASTIC CROSS SECTIONS

The main goal of this paper is to provide a reliable calculation for the ionization cross section for the proton-hydrogen system in the intermediate impact energy range 25–100 keV or 1–2 a.u, in impact velocity. We show our results for ionization and support them later by a detailed description of the theory. But as stated in the Introduction, ionization is intertwined with other inelastic processes that are also important in this energy range. It is not possible to accurately describe one without treating all. To support our ionization results, we also show cross sections for excitation to the $2s$ and $2p$ states of the target and capture to $2s$ and $2p$ states of the projectile. Numerical results for reported cross sections are shown in Table I.

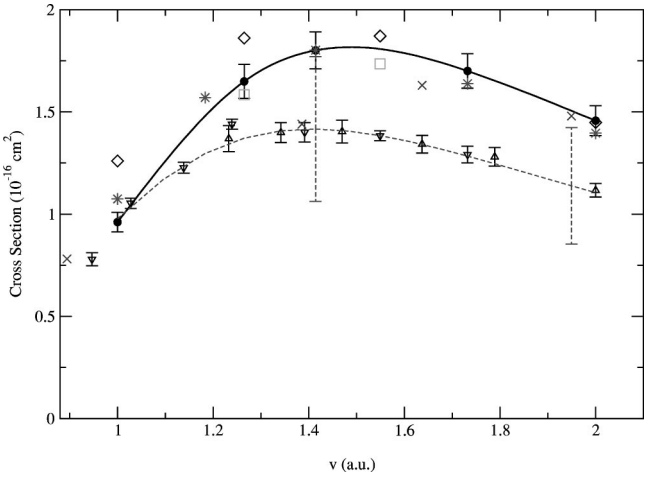

FIG. 1. Comparison of total ionization cross sections with other theory and experiment. solid circles with solid line and error bars, present results; asterisks, Toshima [5]; diamonds, finite difference method by Kolakowska *et al.* [9]; open boxes, Fourier collocation method by Kolakowska *et al.* [9]; up triangles, experiment by Shah *et al.* [3]; down triangles, experiment by Shah *et al.* [4]; ×, experiment by Kerby *et al.* [13]; dashed line is the recommended values from the International Atomic Energy Agency (IAEA). The IAEA rates their data in accuracy class B, 10–25% error. The dashed error bar shows the maximum of that error range, 25%.

A. Ionization

In Fig. 1, we present our total cross section for proton impact ionization of hydrogen. Other recent calculations shown by Toshima [5] and Kolakowska *et al.* [9] represent the state of the art in the close-coupling and lattice methods respectively. The experimental results shown come from Kerby *et al.* [13] and Shah and Gilbody and Shah *et al.* [3,4]. Also shown is the interpolated, recommended values from the International Atomic Energy Agency (IAEA) [23], which are clearly based on the results of Shah *et al.* We estimate uncertainties in our calculation and claim an accuracy of 5% error, putting our cross sections at odds with the values reported by Shah *et al.*

Our calculation of the ionization cross section matches the data of Shah and Gilbody [3] at the low end of our energy range, but we obtain a value 30% higher at the maximum of the ionization cross section. The agreement with the experiment of Kerby *et al.* is slightly better, but there again we have a large discrepancy near the maximum of the cross section. The curve from the IAEA is classified as accuracy category B, 10–25 % error, significantly larger error than reported by Shah *et al.* The error bars of the present calculation does overlap with the 25% error bars drawn in Fig. 1. One of the main difficulties in producing the experimental cross sections is to determine the ratio of atomic hydrogen to molecular hydrogen in the gas target. In the case of Refs. [3,4] the data is normalized to the Born approximation at impact velocity of $v=7.75$ a.u. The validity of the Born approximation, even at that high an impact velocity, is an open question [5,24]. Normalization issues aside, the shape of our calculation does not fit with that of Shah *et al.*

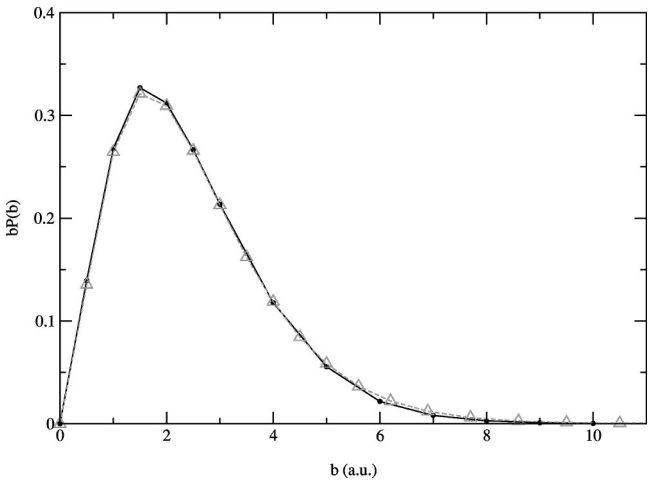

FIG. 2. Comparison of weighted probabilities, $bP(b)$ for ionization between present calculation, solid circles with solid line, and Toshima [5], up triangle with dashed line, for an impact energy of 50 keV ($v=1.414$ a.u.)

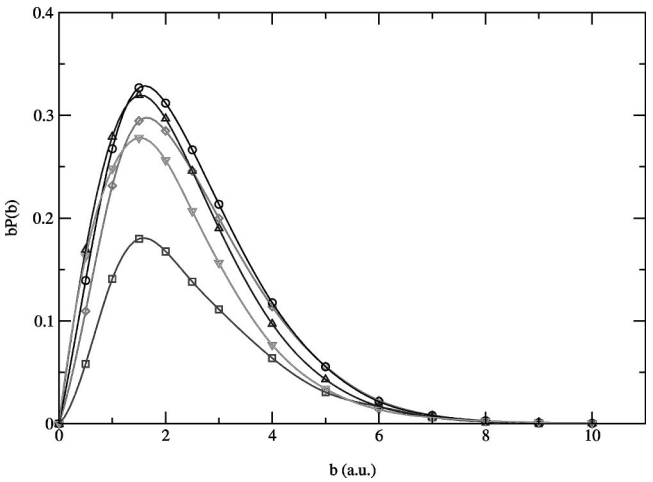

FIG. 3. Weighted probabilities of ionization, $bP(b)$, for all energy points calculated for this article: line with squares 25 keV ($v=1$), line with diamonds 40 keV ($v=1.265$), line with circles 50 keV ($v=1.414$), line with up triangles 75 keV ($v=1.732$), and line with down triangles 100 keV ($v=2$).

The ionization cross section of the present calculation compares better with other recent theoretical calculations than with the reported experimental data. Our calculation agrees with both reported points from the Fourier collocation calculation of Kolakowska *et al.* [9], but their numbers from the finite difference method are about 30% higher at impact velocity $v=1$ a.u. Ref. [9] does not, however, express a lot of confidence in their ionization cross section due to the indirect way in which it is determined, citing the difference between their own Fourier collocation and finite difference calculations. The present ionization cross section agrees best with the close-coupling calculation of Toshima [5]. The only significant disagreement is at impact velocity 1 a.u., where Toshima's value is 11% higher than our cross section for impact ionization. At 50 keV ($v=1.414$), the present calculation agrees with Toshima's number to within 1%. Even at the level of impact-parameter dependence, see Fig. 2, our computed probability of ionization fits well with Toshima's. We also show the impact-parameter dependence of the ionization probability for the other energies we calculated in Fig. 3. We come back to a more detailed discussion of the comparison between our results and the other theories after presenting our theoretical framework.

B. excitation and capture

Considering the scatter in the various results for the ionization cross section, we offer additional support for our calculation by showing its results for excitation and charge transfer. In Fig. 4, we compare our cross section for excitation to $2p$ with experimental results of Detleffsen *et al.* [25] and Barnett [26] in addition to the theoretical calculations of Toshima [5] and Schultz *et al.* [27]. Our calculation is consistent with the experiment for impact velocities in the range of $v=1$–1.3 a.u. and then once again at $v=2$. The present calculation shows smooth behavior between those limits, while the experiment of Ref. [25] shows a rapid increase between impact velocities 1.3 and 1.4 a.u.; such structure is difficult to understand for these intermediate impact energies. The close-coupling calculations also are higher than the present calculations in the middle of our energy range, but not as high as the experiment by Detleffsen *et al.* The lattice results come in slightly above the close-coupling results at intermediate velocities but they agree with each other at low energy. We remark that the impact-parameter range covered in the present calculation goes to $b=10$ a.u., which is sufficient for ionization but falls a little short for excitation to the $2p$. We extrapolated the impact-parameter dependence of the excitation probability, and the extrapolated piece contributes as much as 6% , at $v=2$, to our reported cross sections. (The

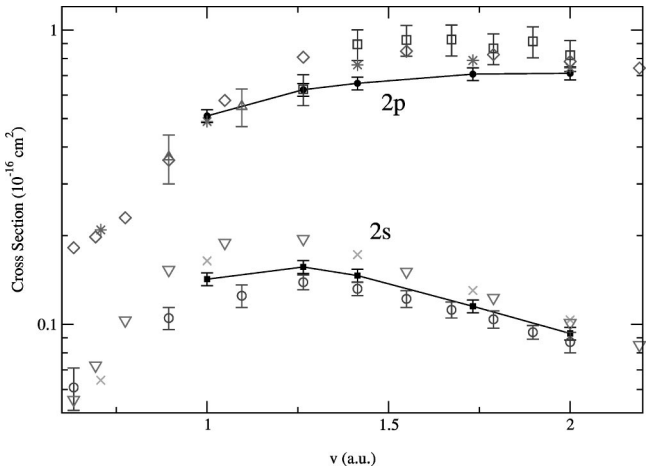

FIG. 4. Comparison of excitation cross section with experiment. $H2s$ excitation: solid squares with lines and error bars, present calculation; crosses, Toshima [5]; down triangles, Schultz *et al.* [27]; open circles, Higgins *et al.* [28]. $H2p$ excitation: solid circles with lines and error bars, present calculation; asterisks, Toshima [5]; diamonds, Schultz *et al.* [27]; open squares, Detleffsen *et al.* [25]; up triangles, Barnett [26].

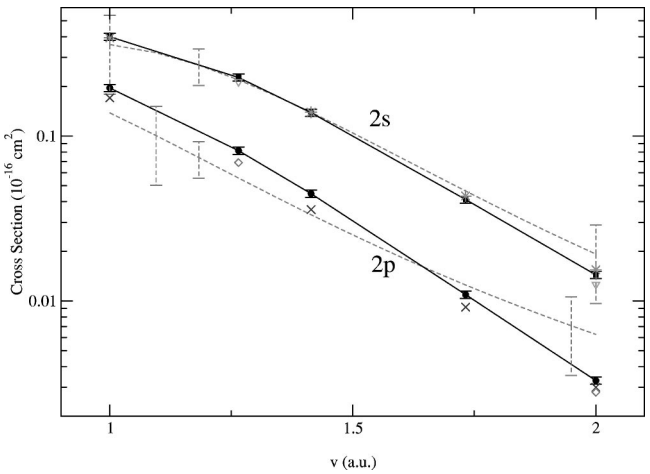

FIG. 5. Comparison of capture cross section with recommended numbers from the International Atomic Energy Agency (IAEA). $H2s$: solid squares with lines and error bars, present calculation; asterisks, Toshima [5]; down triangles, Kolakowska *et al.* [29]; dashed line, IAEA. $H2p$: solid circles with lines and error bars, present calculation; crosses, Toshima [5]; diamonds, Kolakowska *et al.* [29]; dashed line, IAEA. Outer error bars on the IAEA curve represent the IAEA's maximum error bar, and the interior error bar represents IAEA's minimum error bar.

extrapolated contribution is less than 0.5% at $v=1.414$, where we have the largest discrepancy between theory and experiment.) In Fig. 4, we also show excitation to the $2s$ compared with experiment by Higgins *et al.* [28] and theory by Toshima [5] and Schultz *et al.* [27]. The lattice results match well with the close-coupling calculation for intermediate energy. Our calculation agrees with the experiment to within experimental and theoretical error bars, while the close-coupling calculation falls outside the experimental error bars at intermediate impact velocities.

Turning to the capture cross section, we show in Fig. 5 our results for capture to $2s$ and $2p$ compared with recommended values from the IAEA, calculations by Toshima [5] and Kolakowska *et al* [29]. The IAEA classifies its $2s$ capture as accuracy category C/E and $2p$ capture as accuracy category C: C means 25 to 50% error and E is more than 100% error. In the figure, 50% error bars are put on the IAEA data at the endpoints, and a 25% error bar is shown on one interior point. The capture to the $2p$ agrees with the present calculation to within prescribed accuracy. The agreement between the two sets of numbers is even better for capture to the $2s$. Our calculation is even within the 25% error bar of their prescribed numbers. Moreover, we have agreement over the whole impact velocity range where both capture cross sections drop more than an order of magnitude. The close-coupling results match with our $2s$ capture cross section but not for $2p$ capture, which lies outside our error bars. The lattice calculations for $2s$ capture track the present and close-coupling results, but the lattice results for $2p$ capture are again below the present calculation and appear to agree with the close-coupling results. In any case, all three theoretical calculations fit with the IAEA recommended data. The fact that the TCMSD calculation gives reasonable cross sections for the inelastic process that are weaker than ionization gives us additional confidence in our reported ionization cross sections.

III. THE THEORETICAL FRAMEWORK

We review here the two-center momentum space discretization (TCMSD) method, because its implementation has evolved since the original articles [19,20]. Also, the emphasis of this article is to provide accurate numbers, so a detailed description of TCMSD with a critical assessment of its strengths and weaknesses is in order.

The proton on a hydrogen collision system is viewed in the standard semiclassical framework, where the internuclear motion is classical and the electron is treated fully quantum mechanically. Moreover, we assume rectilinear motion for the projectile center with constant velocity $\vec{v}$ and impact parameter $\vec{b}$. The time-dependent Schrödinger equation, written in the target frame, for an electron in the field of the two protons is

$$i\frac{\partial}{\partial t}\psi(\vec{r},t)=\left(-\frac{1}{2}\nabla^2-\frac{1}{|\vec{r}|}-\frac{1}{|\vec{r}-\vec{R}|}\right)\psi(\vec{r},t),\quad \vec{R}=\vec{v}t+\vec{b}. \tag{1}$$

The coordinate system is the natural frame, where the projectile velocity $\vec{v}$ is along the x axis, the impact parameter is along the y axis, and the z axis is perpendicular to the collision plane. Atomic units are used throughout. The details on the two-center momentum space discretization (TCMSD) method, employed to solve Eq. (1), are presented in Ref. [19]. Here, we restate the form of the electronic momentum space wave function, give a brief account of how the time-dependent wave function is found, and discuss the calculational parameters used to solve Eq. (1). We describe at length how bound-state and ionization amplitudes are derived from the time-dependent wave function.

A. Wave-function propagation

The electron wave function in the ion-atom collision is represented by a two-center expansion in momentum space

$$\Phi(\vec{p},t)=\sum_{l,m}\tilde{T}_{l,m}(p,t)Y_{l,m}(\hat{p})+e^{-i(\vec{p}\cdot\vec{R}-1/2v^2t)}\times\sum_{l,m}\tilde{P}_{l,m}(q,t)Y_{l,m}(\hat{q}),\quad \vec{q}=\vec{p}-\vec{v}, \tag{2}$$

where the spherical harmonic $Y_{l,m}$ is defined with respect to each center in the momentum space expansion. We use the real form of the spherical harmonics with the convention that positive values of m refer to $\cos m\phi$ and negative values of m refer to $\sin m\phi$. The phase factor in front of the second sum on the right of Eq. (2) is the plane-wave electron translation factor in the momentum space. We have carried out a partial wave expansion on each center and the radial functions $\tilde{T}_{l,m}(p,t)$ and $\tilde{P}_{l,m}(q,t)$ are in turn expanded in B splines:

$$\tilde{T}_{l,m}(p,t)=\sum_{i=1}^{N} c_i^{lm}(t)\tilde{B}_i(p)+c_1^{lm}(t)f_l(p_{min},p) + c_N^{lm}(t)g_l(p_{max},p). \quad (3)$$

The B-spline expansion covers a range from p_{min} to p_{max}, where p_{min} is nonzero. As in [19], fourth-order basis splines are employed. The knot sequence is repeated at p_{min} and p_{max} in order to have the first and last B spline terminate at unity. We have attached asymptotic pieces to $\tilde{B}_1(p)$ and $\tilde{B}_N(p)$

$$f_l(p_{min},p)=\begin{cases}(p/p_{min})^l & 0\leqslant p<p_{min}\\ 0 & p\geqslant p_{min}\end{cases}, \quad (4)$$

$$g_l(p_{max},p)=\begin{cases}0 & p<p_{max}\\ \dfrac{([(l+1)p_{max}]^2+1)^{2+l}}{p_{max}^l}\dfrac{p^l}{([(l+1)p]^2+1)^{2+l}} & p\geqslant p_{max}\end{cases}. \quad (5)$$

Roughly speaking, f_l takes care of the low-momentum behavior coming from the inner turning point of each partial wave, in configuration space. The function $g_l \approx (p_{max}/p)^{4+l}$ represents the well-known large momentum components of the Coulomb wave function [30]. The particular form of g_l in Eq. (5) is selected to get the lowest n bound state exactly correct for each $l(1s, 2p, 3d,$ etc.), since they are the major players in collisions with ground-state atoms. In any case, the error introduced by this approximation was checked by propagating the $2s$ orbital in time over the duration of a collision with no projectile ion interaction. The resulting probability deviated from unity by 0.02%, much less than other numerical errors. The projectile radial functions have an expansion in q similar to Eq. (3) with the spline coefficients labeled d_i^{lm}.

Substituting Eq. (2) into Eq. (1) gives a set of first-order coupled equations for the expansion coefficients in Eq. (3). The coefficients $c_i^{lm}(t)$ and $d_i^{lm}(t)$ are arrived at through a fourth-order fixed step-size Runge-Kutta integration. The time derivative of the B-spline coefficients at each integration step result from a least-squares fit to $H\psi$ at a set of points that typically outnumber the basis functions by a factor of four. The fit is performed in configuration space after inverse Fourier transformation of the basis functions, $\tilde{B}_i(p)Y_{l,m}(\hat{p})$ and $e^{-i(\vec{p}\cdot\vec{R}-1/2v^2t)}\tilde{B}_i(q)Y_{l,m}(\hat{q})$. The fitting points are arranged as a spherical polar grid about both target and projectile protons. The linear system solved is shown schematically.

$$((A^T)_{K'J}A_{JK})x_K=(A^T)_{K'J}b_J. \quad (6)$$

Products with like indices imply summation. K and K' are indices running through all basis functions, and J is an index running through all the fitting points. The matrix A is a rectangular matrix of all basis functions evaluated at all fitting points. The least-squares method prescribes multiplying through by A^T, providing a square linear system. The vector x_K represents the time derivative of the coefficients, and the vector b_J represents $-iH\psi$ evaluated at the fitting points. The χ^2 of the fit reveals the error of the time derivative of the electron probability density. Once x_K is found, this information is fed into the Runge-Kutta integration, which is checked for accuracy by the wave-function normalization and by reducing the integration step size.

Since the wave-function normalization is not automatically preserved in TCMSD, the deviation of the norm from unity may be used to put error bars on the physical quantities derived from TCMSD propagation. The same cannot be done in close-coupling methods, since the wave-function normalization only reflects accurate time integration and matrix element evaluation, but unit norm does not ensure accurate representation of the wave function itself. In lattice methods, the norm is not preserved at all, as components of the wave function near the boundary of the integration box are masked away [9,27,29]. Close-coupling and lattice calculations must rely on indirect ways to evaluate convergence, such as examining changes in the cross section with respect to varying calculation parameters. Thus, to our knowledge, TCMSD is the only method of solving the time-dependent Schrödinger equation that can directly put error bars on cross sections derived from the propagated wave function.

B. Wave-function analysis

The numerical wave function, having passed the numerical checks, is analyzed to extract the bound-state amplitudes. Previously in Refs. [19–22], we have neglected overlaps between the two centers and performed bound-state projection individually on the target and projectile centers, because we were only interested in the gross features of the ejected electron spectrum. Since we are now interested in obtaining cross sections that are as accurate as possible, it is necessary to project out the bound states on both target and projectile from the whole wave function.

$$a^T_{nlm}(t) = \int_0^\infty F_{nl}(p)\tilde{T}_{lm}(p,t)p^2dp + \int_{V_p} F_{nl}(p)Y_{l,m}(\hat{p})e^{-i(\vec{p}\cdot\vec{R}-1/2v^2t)} \times \sum_{l',m'} \tilde{P}_{l',m'}(q,t)Y_{l',m'}(\hat{q})d\vec{p}, \quad (7)$$

$$\vec{q} = \vec{p} - \vec{v}.$$

$F_{nl}Y_{l,m}$ is the target hydrogen bound state in momentum space and V_p represents volume in momentum space. An analogous formula for the projectile bound-state amplitudes, $a^P_{nlm}(t)$ is simple to write, so we do not show it here. As a technical note, we remark that the numerical integrals in Eq. (7) are actually performed over the radial variable $s=\sqrt{p}$, which allows the same precision with fewer integration points. The momentum space wave function in Eq. (2) contains all bound states of the Coulomb potential, since the bound states *decrease* in size with increasing principal quantum number n. This differs from close-coupling methods, where each bound state is explicitly entered into the calculation, and conventional lattice methods that are limited to $n=3$ [9,27,29] since bound states *increase* in size proportional to n^2 in configuration space.

For the present purposes, we are interested in finding the probability of ionization as opposed to the distribution of ejected electrons. Thus, we do not attempt to construct the continuum part of the wave function, but instead we write the probability for ionization as the total probability minus the bound states on target and projectile

$$P_{ion}(b) = N(b) - \sum_i (|a^T_i(t_f)|^2 + |a^P_i(t_f)|^2); \quad (8)$$

$$N(b) = \int_V \Phi(\vec{p},t_f)^*\Phi(\vec{p},t_f)d\vec{p}.$$

The index i runs through all bound-state probabilities. The quantities, of course, are taken at their final value $t=t_f$. The target and projectile amplitudes are grouped in the same sum, because in all cases, the same harmonic expansion was used on both centers. It is not possible to take the sum over bound states up to $n=\infty$, so instead, we compute Eq. (7) for bound states through $n_{max}=5$ for impact-parameter $b\leqslant 5$. (For larger impact-parameter $n_{max}=3$ since amplitudes for higher n are too small.) To extrapolate to higher n, we use the $1/n^3$ scaling of the bound-state probabilities

$$|a_n|^2 = |a_{n_{max}}|^2(n/n_{max})^3 \quad \text{for} \quad n>n_{max}. \quad (9)$$

The extrapolated values are entered into the sum in Eq. (8).

The error of the bound-state probabilities is, to first order, the same as the relative error on the wave-function norm. In actuality, the relative error increases slowly with n, since the higher the excited state is, the fewer radial B splines there are to represent it (as the radial momentum collapses to zero as n increases). Thus, the highly excited states are at the mercy of scatter in just a few basis functions. There is also an additional error on the bound-state probabilities due to stopping the TCMSD propagation at a finite time, discussed more below. The error in $P_{ion}(b)$ is the absolute error in the wave-function norm, since we obtain it by subtracting the bound-state probabilities from the total wave-function probability. We estimate the error in the total ionization cross section by computing a relative error at each impact parameter $\epsilon(b) = |1-N(b)|/P_{ion}(b)$. The effect of this error on the total cross section for ionization is about in the range of 3–3.5 %. An additional error comes from the extrapolation of the bound-state probabilities to $n=\infty$, resulting in additional 1–1.5 % error. Cross sections for bound-state processes will have less error from inaccuracy of the propagation, but more error due to stopping at a finite time. Thus, we put error bars of 5% on all our calculated cross sections, including the excitation and capture cross sections to $n\leqslant 2$.

C. Parameters of the TCMSD calculation

We discuss the actual parameters used in the calculation. Selection of the proper radial grid on which the B splines are defined and a suitable number of harmonics about each proton is critical for a valid calculation. In addition, an appropriate set of fitting points must be chosen, avoiding linear dependence difficulties within the basis set. For the current paper, three different basis sets were tested: set A, specialized for low-impact parameter collisions, set B, for large impact parameter, and set C from our earlier work [20]. After specifying the parameters of each basis set, we show a comparison of all three sets for an impact energy of 25 keV at the intermediate impact-parameter $b=2.0$.

Since the two-center nature of the ion-atom collision is taken into account already by the expansion about each nucleus, much of the numerical effort goes toward solving for the radial functions. Thus, in all cases we take $l_{max}=2$. Since the quantization axis is chosen to be perpendicular to the collision plane, the odd-parity states are never populated due to the even parity of the initial s state. Thus, six spherical harmonics cover all partial waves up to and including $l=2$. In radial momentum, p_{min} is fixed at 0.01 a.u., but p_{max} varies in each basis set and in some cases it varies with l. In general, one expects larger momentum to be important for lower l, since low l partial waves extend to smaller r in configuration space, where the kinetic energy is larger.

The specific basis sets are chosen as follows. Set A: The B-spline knot points were selected at intervals of 0.05 between 0.01 and 4.01 a.u. specifying 83 radial B splines. The same radial set was used for all partial waves, because we found that high momentum plays an important role for s, p, and d partial waves in close collisions ($b\leqslant 1$). Totaling the harmonics and corresponding radial B splines, set A is composed of 996 (12×83) elements. Set B: For larger impact parameter, the radial momentum functions turn out to be smooth functions aside from a phase factor, $\exp(-ip^2t/2)$, multiplying the continuum component (see Fig. 9 in Sec. IV C). Thus, we design a knot sequence with relatively large

spacing for low momentum, but then for high momentum the interval spacing *decreases*. The knot points follow the following formula:

$$p_i = \begin{cases} 0.07i + 0.01 & 0 \leqslant i \leqslant 30 \\ \sqrt{2.11^2 + (i-30)(p_{max}^2 - 2.11^2)/K} & 30 < i \leqslant 30+K \end{cases}. \quad (10)$$

We use a wider spacing of 0.07 for the knot points between 0.01 and 2.11. For large momentum, $p > 2.11$, the formula in Eq. (10) gives constant intervals in p^2 so that the oscillations of the $\exp(-ip^2t/2)$ phase factor are equally well represented. For the *s*-wave $K=39$ intervals are necessary in the second part in order to reach $p_{max}=4.0$ and at the same time have the first interval after $p=2.11$ be close to 0.07. With Eq. (10) $p_{31}-p_{30}=0.069$ and the last interval is $p_{69}-p_{68}=0.037$. The big savings comes in the partial waves *p* and *d*, where *K* is only 15 reaching $p_{max}=3.0$. The number of *B* splines in the *s*, *p*, and *d* partial waves are 72, 48, and 48, respectively. The total number of basis elements is 624, a reduction of more than a third from set A. Set C: The final basis set has equally spaced *B* spline knots as does set A, and likewise the interval is chosen to be 0.05 a.u. in momentum. The difference is that p_{max} is taken to be 4.01, 2.51, and 2.01 for the *s*, *p*, and *d* partial waves, respectively. The number of basis elements for this case is 636, comparable in size to set B.

Determining the proper set of configuration space fitting points is also important for having a stable propagation of the electronic wave function. The fitting points are arranged as a spherical polar grid about both target and projectile protons. In the azimuthal angle ϕ, we choose six angles at equal intervals of $\pi/3$ radians except when $\theta=0$ due to the degeneracy of ϕ on the *z* axis. Only three values of θ are selected: $\theta=0$, $\pi/5$, and $2\pi/5$. The other values of θ, $3\pi/5$, $4\pi/5$, and π, are redundant because of reflection symmetry; recall that we use the natural frame. Thus, there are a total of 13 angular fitting points on each center to uniquely determine six harmonics on each proton. As a guide to setting the radial fitting points, one may think in terms of the inverse relationship between interval size and stepsize between Fourier space and configuration space. Take the largest basis, set A, to start with. The interval spacing is 0.05 a.u. in momentum space, so one expects that the fitting points should extend to $2\pi/0.05$ or ≈ 126 a.u. in configuration space. Likewise, the highest-spatial frequency is given by $2\pi/p_{max}$ or ≈ 1.57 a.u., and one would expect to have at least two points per oscillation. By trial and error we settled on the following set of radial fitting points:

$$r_i = 0.6i + 0.5 \quad \text{for} \quad 0 \leqslant i \leqslant 100,$$

$$r_i = 4.0(i-100) + 0.5 \quad \text{for} \quad 100 < i \leqslant 115. \quad (11)$$

The radial fitting points start at $r=0.5$, end at $r=120.5$, and have a high-resolution grid up to $r=60.5$. The number of fitting points is 3016 ($2\times13\times116$), and the same set of fitting points is used to determine sets *A*, *B*, and *C*. An important point to have stable propagation of the wave function is to weight the fitting points in the radial direction by r^2, since the number of angular points remains at 13 no matter how large *r* is, yet the spherical shell they cover grows with r^2. In any case, with this set of fitting points basis set A is over determined by a ratio of 3 to 1, while sets B and C are overdetermined by close to 5 to 1.

TABLE II. Comparison of TCMSD calculations with basis sets A and B (see text) for a 25 keV collision at impact parameter $b=2.0$ a.u. Probabilities for bound states and electron ejection are compared at $vt=25.2$ a.u. Columns 1 and 2 show probabilities from sets A and B, respectively. Column 3 gives the percent difference of probabilities arrived at through sets A and B.

	set A	set B	% diff.
Norm	1.0052	1.0069	-
P_{ion}	0.083 86	0.084 25	4.63%
Targ. $1s$	0.479 66	0.488 05	1.72%
$2s$	0.009 91	0.009 65	2.62%
$2p\sigma$	0.011 94	0.012 37	3.48%
$2p\pi$	0.016 33	0.016 77	2.62%
Proj. $1s$	0.301 34	0.293 39	2.64%
$2s$	0.041 91	0.041 84	0.17%
$2p\sigma$	0.000 78	0.000 83	5.66%
$2p\pi$	0.008 77	0.008 69	0.91%

D. Comparison of basis sets A, B, and C

We compare the three basis sets for a 25 keV collision at impact-parameter $b=2.0$. As stated above, the main criterion, determining how good a TCMSD calculation is, is the preservation of the total wave-function norm. Evaluating the norm of sets A, B, and C at the final time, $t_f=25.2$, gave values of 1.0052, 1.0069, and 1.0160, respectively. Set A, clearly, is expected to be the best since it has the most basis elements. Set B, however, is significantly better than set C with the norm deviating from unity by 0.7% as opposed to 1.6% for set C. We have also checked this conclusion for other collision parameters. We remark that despite the differences in sets A, B, and C, all three calculations show similar ejected electron momentum distributions. Table II compares the probabilities for, capture, excitation, and ionization from sets A and B. The percent difference between the two calculations is shown also to see if these results are consistent with the estimated error of 5%. Indeed, the probabilities for the bound states and ionization vary in the range of 5% or less. Only the capture to the $2p\sigma$ shows a fractional difference greater than 5%, but this particular capture channel is very weak. Capture to $2p$ still only varies by about 1% between the two calculations. For the cross sections shown in this article, set A was used for $b \leqslant 2.0$ and set B for $2.0 < b \leqslant 10.0$.

E. vt dependence

Ideally, to establish the probabilities of various processes in the ion-atom collision, one would like to propagate the electronic wave function to $t=\infty$. In reality, this is not pos-

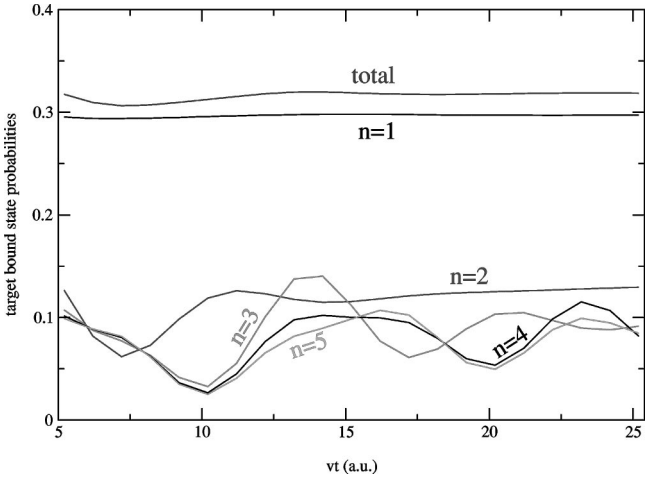

FIG. 6. Target *s*-wave bound-state probabilities, calculated by Eq. (7), as a function of vt. v is the projectile velocity and t is the time measured from closest approach. The collision energy is 25 keV ($v=1$) and the impact parameter is 1.5 a.u. All probabilities have been multiplied by n^3 except for the curve representing the sum of all the bound-state probabilities. The curves are labeled by their corresponding n values. The curve labeled ''total'' represents the sum of the probabilities for all bound states of the target *s* wave.

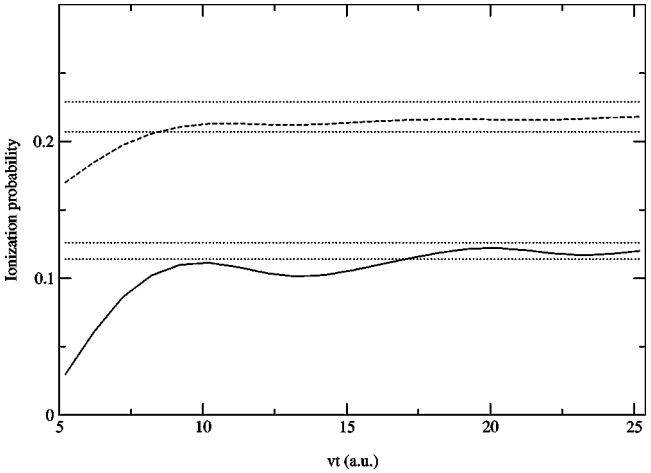

FIG. 7. Probability for ionization, calculated by Eq. (8), as a function of vt. v is the projectile velocity and t is the time measured from the closest approach. The impact paramter is $b=1.5$, and the solid line is the result for a 25 keV ($v=1$) collision and the dashed line is for the 50 keV ($v=1.414$). The dotted lines are placed at 5% in either direction of the final values.

sible. Accordingly, we demonstrate that our ending point of $vt_f=25.2$ is sufficient to establish the bound-state and ionization probabilities, to within 5%, for collisions in the range of 25–100 keV.

In Fig. 6, we show bound-state probabilities, arrived at through Eq. (7), for the *s* wave on the target proton during a 25 keV collision at $b=1.5$ a.u. The probabilities have been multiplied by n^3 to allow all levels to be plotted on the same graph and to demonstrate the $1/n^3$ scaling. The probabilities for $n=1$ and $n=2$ have clearly stabilized by $vt=25.2$, but higher n's have not. One may see a decrease in the amplitude of the oscillations of the $n=3$ probability, but the $n=4$ and 5 will not stabilize until much later. The oscillations at higher n, however, do not affect our analysis very much since their probabilities are so small. Note that there is hardly any vt dependence in the sum of all n-level probabilities. Looking at the ''final'' values for $n=3$, 4, and 5, one sees that the $1/n^3$ scaling holds reasonably well. The contribution to the ionization cross section from the extrapolated bound states, $n\geqslant 6$ enters at the level of about 3–4 %. The error in the extrapolation is rather large, not because of breakdown in the $1/n^3$ scaling, but because the $n=5$ probability is still oscillating at $vt=25.2$. The amplitude of this oscillation is about a third of the $n=5$ probability. Thus, the error in the ionization cross section, coming from the bound-state extrapolation, is 1–1.5 %.

In Fig. 6 we have only shown a small subset of the bound states involved in calculating the ionization cross section. Do the other bound states' vt dependence affect the ionization probability? What about overlap between bound states on both centers? The easiest way to answer these questions is to show the probability for ionization as a function of vt. Since the normalization of the calculations presented here is preserved to 0.5%, any larger variations with vt must come from the above-mentioned questions. In Fig. 7, we plot the probability for ionization for a 25 and 50 keV collision at impact-parameter $b=1.5$ a.u. The dotted lines are drawn in at 5% on either side of the final value. The ionization probability at 25 keV does not enter the claimed error range until $vt=17$ a.u., while the 50 keV ionization probability has already reached 95% of its final value at $vt=7$ a.u. There is a slight oscillation in P_{ion} for the 25 keV calculation that undoubtedly stems from the oscillations seen in the high-n bound states in Fig. 6, but the curve remains within the prescribed limits. We did not attempt to evaluate an ionization cross section for impact energies less than 25 keV due to insufficient range in vt.

IV. DISCUSSION

Having shown results for the ionization cross section and having described exactly how we arrive at our numbers, we now discuss how well TCMSD, close-coupling [5], and lattice [9] approaches meet the challenges of the proton-hydrogen system at intermediate impact energies. Specifically, we talk about convergence in partial waves, radial momentum range, and radial momentum resolution. Theories converged on these three criteria are completely converged calculations. The TCMSD method has a large advantage over other methods on the last point – the momentum resolution.

A. Partial wave-convergence

For the TCMSD calculation, we have included partial waves up to $l=2$. We do have, however, two strong pieces of evidence that this is sufficient. (1) For the calculations that we have performed, even the $l=2$ harmonics receive a small fraction of the total wave function. (2) As stated before, the TCMSD method does not automatically preserve the wave-function norm. If a portion of the wave function were lost to the higher harmonics, this would show up as a deviation of

the norm from unity. The lack of higher partial waves could in fact be the reason why the norm is preserved to 0.5% and not better.

The lattice calculation has no real limitation here, since all partial waves are implicitly contained in their three-dimensional Cartesian grid. For two-center close-coupling, the question of the necessary number of partial waves has been an interesting issue for many years, see, for example, Kuang and Lin [7,8]. One would like to have pseudostates representing the continuum on both target and projectile centers, but this may lead to false oscillatory structure in the resulting inelastic cross sections [7,8]. The conclusion of Refs. [7,8] was to put only pseudostates on one center and go to partial waves up to and including $l=5$ on that center. Toshima, however, showed in Ref. [5] that $l=5$ is not even sufficient to achieve convergence of the ionization cross section, when pseudostates are placed on one center. Reference [5] did show that the convergence in partial waves was very rapid if pseudostates were included on both centers (in accordance with the TCMSD calculation), and furthermore, the false oscillation problem disappears if pseudostate energies are dense enough [31].

B. Momentum range

For all the individual runs of the TCMSD calculation, the normalization is preserved to close to 0.5% except for one case; for the $v=2.0$ collision at an impact-parameter $b=0.5$ the final wave-function norm comes in at 97.4%. This loss of norm does not affect the total cross-section calculation much, since the probability of ionization at $b=0.5$ is over a third. So the dip in the norm causes the error to spike to 8% for this one point, and we maintain the 5% error on the total cross section. It is, however, important to understand why this happens to know the limitations on the theory.

The reason for the loss of norm may be traced to the necessity of representing high-momentum components on the projectile for collisions at high-impact velocity and low-impact parameter. Figure 8 shows the projectile s, $p\sigma$, and $p\pi$ momentum radial functions at $vt=0.2$, just after the projectile has reached closest approach. At this early a point, $vt=0.2$, along the projectile trajectory the contribution to the projectile component of the wave function comes mainly from the ground-state hydrogen target atom. Accordingly, the projectile radial functions display a broad maximum near $p=2$ a.u., since the target wave function in momentum space is separated from the projectile center by 2 a.u. Furthermore, the broadness of the peak reflects the wide initial momentum distribution of the target electron. The target atom also has a larger overlap with the projectile $p\sigma$ wave, explaining why our $p\sigma$ radial momentum amplitude is larger than the $p\pi$ amplitude. A part of the peak at $p=2$ probably has a connection with the binary encounter mechanism, but the projectile velocity is too slow to clearly separate out the binary encounter component. The maximum radial momentum represented by B splines in the TCMSD calculation is $p_{max}=4$, and the tail of the projectile momentum distribution is not so small at this momentum for $v=2$. This problem makes a two-center expansion difficult for high velocity. In any case, the current set of TCMSD parameters allows collision energies up to 100 keV.

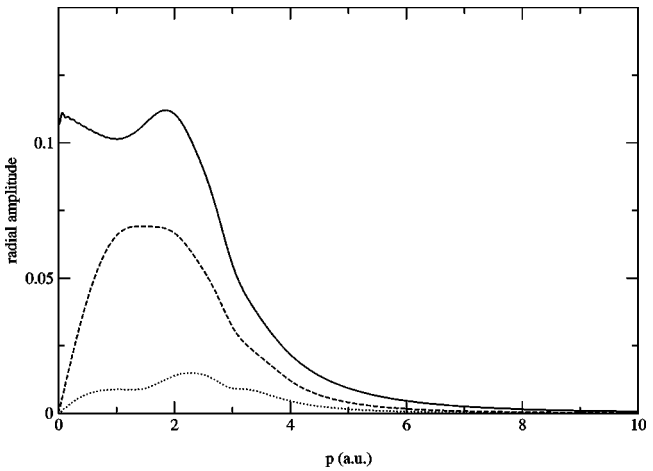

FIG. 8. The amplitude of momentum space radial functions on the projectile immediately after closest approach $vt=0.2$, where the collision velocity is $v=2$ and t is time measured from the closest approach. The impact parameter is $b=0.5$ a.u. The solid line represents the s-wave amplitude, the dashed line is the $p\sigma$ amplitude, and the dotted line is the $p\pi$ amplitude. $p\sigma$ and $p\pi$ are the real form of p-orbitals aligned, respectively, parallel and perpendicular to the projectile velocty in the collision plane.

The lattice calculation must have these large momentum components represented, since the ground-state orbital is represented numerically, which requires momentum components up to at least 10 a.u. The $p=2$ peak in the projectile radial momentum corresponds roughly to a pseudostate energy of 2 a.u. in the projectile frame (from evaluating $p^2/2$). The calculation of Ref. [5] included pseudostates up to 4–5 a.u. in energy. Thus, it is no surprise that we have agreement between TCMSD, close-coupling, and the lattice method at $v=2$ a.u. in Fig. 1.

C. Momentum resolution

At the lower end of the impact velocity range $v=1$, TCMSD, close-coupling, and the lattice method differ considerably in their reported ionization cross section. This variation may be traced to the differences in radial momentum resolution. The TCMSD radial momentum resolution is 0.05 or 0.07 a.u., depending on whether one is using basis set A or B. A rough idea of the close-coupling momentum resolution may be arrived at by taking the square root of twice the pseudostate energy $\sqrt{2E}$. Thus, for low-energy pseudostates the calculation by Toshima [5] has a resolution of 0.11 a.u. For the high end of the pseudostate spectrum, the resolution is considerably worse, ≈ 0.8 a.u. The momentum resolution of the lattice calculation is actually determined by the size of the Cartesian grid in configuration space, due to the inverse relation between coordinate space and Fourier space. The calculation of [9] applies a masking function at the boundary of a box going from -30–30 a.u. The action of the masking function on the configuration space wave function is the same as convolving the momentum space wave function with the Fourier transform of the masking function. Thus,

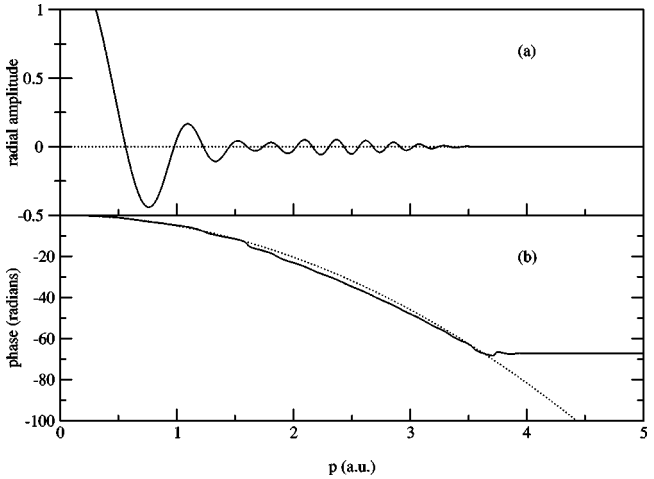

FIG. 9. The target momentum space radial function for the s wave of the 25 keV collision at impact parameter $b=1.5$ and at a time $t=10.2$ a.u. after closest approach. (a) The solid line represents the real part of the target radial s wave after projecting out the $1s$ bound state. The ripples in the total radial function result from a $\exp(-ip^2t/2)$ phase in the continuum interfering with the bound part, which is mainly just the $1s$ state. (b) The solid line is the phase derived from the real and imaginary part of the radial s wave after having projected out the $1s$ bound state. The dotted line is the argument of the expansion phase, $-p^2t/2$ at $t=10.2$ a.u..

their momentum resolution is $2\pi/60$ or 0.1 atomic unit, since any finer detail would be washed out by convolution. The TCMSD calculation has a factor of two better momentum resolution than any other previous theory applied to proton-hydrogen collisions.

Why is momentum resolution important at low-impact velocity? The start of the response to this question is seen in Fig. 7. The slower collision takes longer to stabilize than the higher-velocity collision; one must represent the electronic wave function to at least $vt=17$ ($t=17$) a.u. in the 25 keV case while $vt=7$ ($t=5$) is sufficient for 50 keV collision. A scaling law for the dependence of ionization on internuclear separation [22], predicts that the internuclear separation at which ionization stabilizes is proportional to v^2; thus, one expects that the 25 keV collision needs to be propagated twice as far in vt as the 50 keV case (or $2\sqrt{2}$ longer in time). During the longer stabilizing time, the wave function for the 25 keV collision becomes more complicated. Figure 9(a) shows the real part of the momentum radial function for the target s wave at $vt=10.2$ a.u. after the $1s$ bound state has been projected out. Thus, this radial function represents mostly continuum levels. Note that the radial function displays quite a few oscillations. The cause for these oscillations was identified in Refs. [20,32]. The ejected component of the wave function exhibits, to first order, a free expansion in configuration space. This means that the ejected electron component of the momentum space wave function evolves in time similar to $\exp(-ip^2t/2)$. Extracting the corresponding phase, one can see that it matches well with $p^2t/2$ in Fig. 9(b) for $t=10.2$ a.u. [The second part of the set B knot point grid was designed to deal with this phase better, see Eq. (10)]. As time increases, this phase factor creates more of a problem, since it is proportional to time. The 25 keV ($v=1.0$) collision took more than three times the amount of time to reach its final probability values than the 50 keV ($v=1.414$) collision. Hence, it is clear why the theories, which agree well at 50 keV, diverge from each other at 25 keV. Of the three theories shown in Fig. 1, TCMSD is the best equipped to deal with the radial phase oscillations because of its superior momentum resolution.

V. FUTURE OUTLOOK

The immediate goal of this paper is to provide accurate total ionization cross sections for the proton-hydrogen system at intermediate impact energy. But an equally, if not more, important goal is to show the way to better models of ion-impact ionization. The lattice calculation is enormous, employing 27 000 000 ($300\times300\times300$) grid points. Direct generalization of this method to more complicated systems such as ion-impact ionization of molecules is out of the question. The two-center momentum space discretization and close-coupling methods are more compact calculations with basis sizes of 500 to 1000 elements, but still these calculations are large. From the discussion of the radial phase above, it is clear that one can do better. Already, one can see that the wave-function representation in TCMSD is lopsided. Only 12 harmonics are necessary, six on each center, to cover the wave function. On the other hand, as much as 80 radial B splines were necessary to describe the radial momentum behavior. We have just showed that free expansion of the ejected electron component of the wave function is responsible for ripples in the radial momentum. Thus, the next step for future theory should be to take care of this expansion phase analytically allowing a reduction in the number of basis functions and propagation of the wave function to much larger times.

There already has been some theoretical work addressing the analytical treatment of the ejected electron expansion. In 1985 Solov'ev and Vinitsky [33] proposed solving ion-atom collision in coordinates where the internuclear separation is scaled to unity. Such a scaling confines the ejected electron cloud and introduces a phase factor $\exp(ivr^2/R)$ which is the configuration space analog of the momentum space phase factor, $\exp(-ip^2t/2)$ discussed above. A two-state model based on the Solov'ev scaling has been developed for proton-hydrogen collisions [34], but it has not provided total cross-section values. Illescas and Riera [35] have proposed to apply the expansion phase factor $\exp(ivr^2/R)$ as a generalized translation factor without scaling the coordinate space of the ion-atom collision. Recently, Sidky and Esry [36] have proposed two solutions to the general problem of describing ionization in any atomic process: (1) writing a general scaled time-dependent Schrödinger equation akin to the Solov'ev scaling but avoiding its inherent singularities; (2) solution of the time-dependent wave equation with a combination of stationary Gaussians and Gaussian wave packets. Reference [36] solved a one-dimensional model problem demonstrating their methods. As of yet, there has been no attempt to solve the full proton-hydrogen system taking into account analytically the basic motion of ejected electron component, but the

results presented in this article clearly show that accounting of the expansion is a necessary step toward an improved theory of ion impact ionization.

In summary, we have provided total cross-section calculations for proton impact ionization of hydrogen at an energy range where this process is the most important, 25–100 keV (1–2 a.u. of velocity). The results are in accord with other recent theoretical calculations except at the low-impact velocity end, $v=1$ a.u. Our two-center momentum space discretization method has allowed us also to estimate error bars of 5% . The present calculation gives a maximum cross section of 1.82×10^{-16} cm^2, while the accepted experimental results measure a maximum of 1.42×10^{-16} cm^2. Our value for the maximum ionization cross section is 22% higher than the experimental value, which considering the error bars claimed on both numbers, constitutes a disagreement.

ACKNOWLEDGMENTS

We thank I. Reiser for careful reading of our manuscript, and N. Toshima for providing us with tables of numbers from his calculations. This work is supported by Chemical Sciences, Geosciences and Biosciences Division, Office of Basic Energy Sciences, Office of Science, U.S. Department of Energy.

[1] F. Gobet, B. Farizon, M. Farizon, M. J. Gaillard, M. Carre, M. Lezius, P. Scheier, and T. D. Märk, Phys. Rev. Lett. **86**, 3751 (2001).
[2] M. E. Galassi, R. D. Rivarola, M. Beuve, G. H. Olivera, and P. D. Fainstein, Phys. Rev. A **62**, 022 701 (2000).
[3] M. B. Shah and H. B. Gilbody, J. Phys. B **14**, 2361 (1981).
[4] M. B. Shah, D. S. Elliott, and H. B. Gilbody, J. Phys. B **20**, 2481 (1987).
[5] N. Toshima, Phys. Rev. A **59**, 1981 (1999); cross sections for excitation and capture were taken from the calculation presented in this paper, but those numbers did not appear in the paper itself.
[6] R. Shakeshaft, Phys. Rev. A **18**, 1930 (1978).
[7] J. Kuang and C. D. Lin, J. Phys. B **29**, 1207 (1996).
[8] J. Kuang and C. D. Lin, J. Phys. B **29**, 5443 (1996).
[9] A. Kolakowska, M. S. Pindzola, and D. R. Schultz, Phys. Rev. A **59**, 3588 (1999).
[10] W. L. Fite, R. F. Stebbings, D. G. Hummer, and R. T. Brackmann, Phys. Rev. **119**, 663 (1960).
[11] H. B. Gilbody and J. V. Ireland, Proc. R. Soc. London **277**, 137 (1963).
[12] J. T. Park, J. E. Aldag, J. M. George, J. L. Peacher, and J. H. McGuire, Phys. Rev. A **15**, 508 (1977).
[13] G. W. Kerby III, M. W. Gealy, Y.-Y. Hsu, M. E. Rudd, D. R. Schultz, and C. O. Reinhold, Phys. Rev. A **51**, 2256 (1995).
[14] W. Fritsch and C. D. Lin, Phys. Rep. **202**, 1 (1991).
[15] B. M. McLaughlin, T. G. Winter, and J. F. McCann, J. Phys. B **30**, 1043 (1997) and references therein.
[16] J. Fu, M. J. Fitzpatrick, J. F. Reading, and R. Gayet, J. Phys. B **34**, 15 (2001).
[17] C. Illescas and A. Riera, Phys. Rev. A **60**, 4546 (1999).
[18] S. Sahoo, K. Roy, N. C. Sil, and S. C. Mukherjee, Phys. Rev. A **59**, 275 (1999).
[19] E. Y. Sidky and C. D. Lin, J. Phys. B **31**, 2949 (1998).
[20] E. Y. Sidky and C. D. Lin, Phys. Rev. A **60**, 377 (1999).
[21] E. Y. Sidky, C. Illescas, and C. D. Lin, Phys. Rev. Lett. **85**, 1634 (2000).
[22] E. Y. Sidky, C. Illescas, and C. D. Lin, J. Phys. B **34**, L163 (2001).
[23] ALADDIN database (www-amdis.iaea.org/aladdin.html) maintained by J. A. Stephens at the International Atomic Energy Agency (www.iaea.org). Data presented here is based on Ref. [26].
[24] N. Toshima, J. Phys. B **25**, L635 (1992).
[25] D. Detleffsen, M. Anton, A. Werner, and K.-H. Schartner, J. Phys. B **27**, 4195 (1994).
[26] C. F. Barnett, Oak Ridge National Laboratory Report No. 6086 (unpublished).
[27] D. R. Schultz, M. R. Strayer, and J. C. Wells, Phys. Rev. Lett. **82**, 3976 (1999).
[28] D. P. Higgins, J. Geddes, and H. B. Gilbody, J. Phys. B **29**, 1219 (1996).
[29] A. Kolakowska, M. S. Pindzola, F. Robicheaux, D. R. Schultz, and J. C. Wells, Phys. Rev. A **58**, 2872 (1998).
[30] B. H. Bransden and C. J. Joachain, *Physics of Atoms and Molecules* (Longman, New York, 1983); see Appendix 5.
[31] N. Toshima, J. Phys. B **30**, L131 (1997).
[32] E. Y. Sidky, in *Applications of Accelerators in Research and Industry*, Proceedings of the Fifteenth International Conference, Denton, Texas, edited by J. L. Duggan and J. L. Morgan (University of North Texas, Denton, 1999).
[33] E. A. Solov'ev and S. I. Vinitsky, J. Phys. B **18**, L557 (1985).
[34] J. H. Macek and S. Y. Ovchinnikov, Phys. Rev. Lett. **80**, 2298 (1998).
[35] C. Illescas and A. Riera, Phys. Rev. Lett. **80**, 3029 (1998); **81**, 1350 (1998).
[36] E. Y. Sidky and B. D. Esry, Phys. Rev. Lett. **85**, 5086 (2000).